Journal of the Physical Society of Japan **90**, 064708 (2021)
https://doi.org/10.7566/JPSJ.90.064708

Spin Wave Excitations in Honeycomb Antiferromagnet $MnTiO_3$

In Yong Hwang[1], Kee Hwan Lee[1], Jae-Ho Chung[1]*, Kazuhiko Ikeuchi[2], V. Ovidiu Garlea[3], Hiroki Yamauchi[4], Mitsuhiro Akatsu[5], and Shin-ichi Shamoto[2,6,7,8†]

[1]*Department of Physics, Korea University, Seoul 02841, South Korea*
[2]*Neutron Science and Technology Center, Comprehensive Research Organization for Science and Society, Tokai, Ibaraki 319-1106, Japan*
[3]*Neutron Scattering Division, Oak Ridge National Laboratory, Oak Ridge, TN 37831, U.S.A.*
[4]*Materials Sciences Research Center, Japan Atomic Energy Agency, Tokai, Ibaraki 319-1195, Japan*
[5]*Department of Physics, Niigata University, Niigata 950-2181, Japan*
[6]*Department of Physics, National Cheng Kung University, Tainan 70101, Taiwan*
[7]*Advanced Science Research Center, Japan Atomic Energy Agency, Tokai, Ibaraki 319-1195, Japan*
[8]*Meson Science Laboratory, RIKEN, Wako, Saitama 351-0198, Japan*

(Received February 24, 2021; accepted April 16, 2021; published online May 21, 2021)

Using inelastic neutron scattering, we investigate the spin wave excitations on the antiferromagnetic $MnTiO_3$ ($T_N = 65$ K), which has the stacked honeycomb structure. At $T = 2$ K, the spin wave energy extends up to 10.7 meV with the zone-center anisotropy gap of 0.8 meV. Whereas the dispersion is also strong along the direction perpendicular to the honeycomb planes, the exchange cancellation causes the magnetic interactions to be effectively anisotropic below T_N. While the spin wave spectrum survives at temperatures above T_N, we find that the magnetic interactions become more anisotropic within the paramagnetic phase. These results suggest that the magnetic interaction in $MnTiO_3$ crosses over from being three dimensional to two dimensional above T_N.

1. Introduction

Recent works on magnetoelectric (ME) effects have opened up new possibilities for manipulating solid state properties via external fields.[1–3] The ME effects appear due to the couplings between electric polarizations (P) and magnetic orders within crystalline solids provided that the symmetries of the two order parameters are compatible with each other. For instance, spin-based ferroelectric polarizations are observed in a wide range of long-range magnetic ordering with broken inversion symmetries based on non-collinear spin structures.[4,5] Whereas such multiferroic P–H coupling is essentially nonlinear involving significant energy losses, certain collinear antiferromagnets can provide dissipationless behavior via the linear ME couplings.[6–9]

$MnTiO_3$ was recently brought into attention owing to its linear ME behavior based on a simple collinear antiferromagnetic (AFM) ordering.[10–13] $MnTiO_3$ has the ilmenite-type crystal structure that belongs to the space group $R\bar{3}$ (No. 148), in which magnetic Mn^{2+} ($S = 5/2$) ions form stacked honeycomb lattices as shown in Fig. 1(a). Contrary to other $ATiO_3$ (A = Fe, Co, Ni) which are ferromagnetic within their honeycomb planes, $MnTiO_3$ establishes a simple AFM ordering below $T_N = 65$ K with spins oriented along the c axis due to the easy-axis anisotropy.[14–17] While the structural inversion centers are bisecting the nearest neighbor bonds of the honeycomb lattice, both in-plane and out-of-plane, the AFM ordering shown in Fig. 1(a) breaks these inversion symmetries. As a result, the ME polarizations appears along the c axis parallel to the spin orientations,[11,12] which is attributed to asymmetric charge distributions in Mn–O bonds due to delocalized Mn 3d holes.[18] This ME polarization flips by 90° into the honeycomb plane simultaneously with a spin flip transition when an external magnetic field above the critical field ($H_c = 6.8$ T) is applied along the c axis.[12,19]

To understand the ME effect and its temperature dependencies, it is important to have reliable information regarding the spin Hamiltonian that determines the underlying AFM ordering and its thermal excitations. Indeed, thermal fluctuations at elevated temperatures are expected to play decisive roles in causing the ME effect in collinear antiferromagnets.[6] Although the Heisenberg exchanges in $MnTiO_3$ were quantitatively estimated more than 30 years ago by analyzing its spin excitations,[20,21] the dynamics at elevated temper-

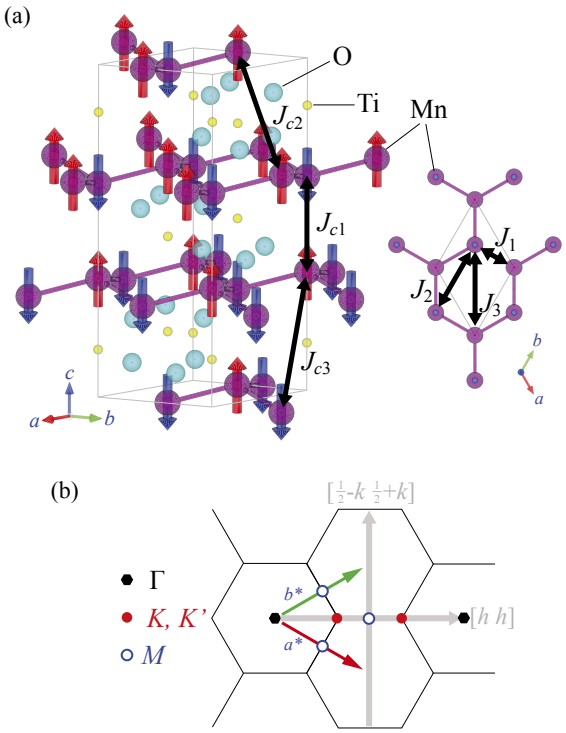

Fig. 1. (Color online) (a) Crystal and antiferromagnetic structures of $MnTiO_3$. Shown on the right is the top view of a single honeycomb plane. The exchange paths considered in this work are marked as doubled ended arrows. (b) The two dimensional reciprocal space of the honeycomb lattice. The solid lines are the Brillouin zone boundaries. The horizontal and vertical gray arrows depict the directions of the cuts plotted in Figs. 3(a), 3(b), and 3(c), respectively.

atures is still unclear. For instance, its Néel temperature is less than one third of the Curie–Weiss temperature at $|\Theta_{CW}| \approx 219$ K in spite of the apparent simple AFM structure.[22] Such a large suppression of the ordering temperature cannot be understood based on its spin Hamiltonian apparently free of significant exchange frustrations.[23,24] Whereas the low dimensionality of the honeycomb planes might further contribute to reducing T_N, the interplanar exchanges were found to be not smaller than a few percent of the intraplanar.[20,21] Furthermore, the critical fluctuations accompanying its AFM phase transition were also found to be largely three dimensional.

In this work, we revisited the spin wave excitations in $MnTiO_3$ and investigated its changes over a wide temperature range across T_N. By fitting the high resolution inelastic neutron scattering (INS) data based on the linear spin wave model, we obtained accurate values of exchange parameters that can excellently describe the spin wave energies over the entire Brillouin zone of the $R\bar{3}$ structure. By observing its temperature dependence, we also find that the magnetic interactions in $MnTiO_3$ essentially becomes two dimensional at $T \gtrsim 80$ K in the paramagnetic phase, which can explain the suppression of long-range AFM ordering at temperatures well below $|\Theta_{CW}|$.

2. Experimental

Large single crystal of $MnTiO_3$ was grown by a traveling solvent floating zone furnace[25] with four halogen lamps (FZ-T-4000-H-II-S-TS, Crystal Systems). A small piece was cut off from the rod for magnetic susceptibility measurements under the external magnetic field ($B = 1000$ Oe) applied parallel to Mn^{2+} spins. Both zero-field-cooled (ZFC) and field-cooled (FC) measurements were performed. The time-of-flight neutron spectroscopy was performed using the BL14-B HYSPEC spectrometer at Spallation Neutron Source Facility of the Oak Ridge National Laboratory.[26,27] The measurements were performed with the crystal oriented either in $hk0$ or hhl scattering geometries. The incident energy was set to be $E_i = 15$ meV with the Fermi chopper frequency of $f = 360$ Hz. At this configuration, the energy resolution is $\Delta E = 0.43$ and 0.16 meV in full-width-half-maximum at the energy transfer of $\hbar\omega = 0$ and 10 meV, respectively. The triple-axis spectroscopy was performed using the SPINS cold neutron spectrometer at NIST Center for Neutron Research. The fixed final energy of $E_f = 3.7$ meV was used along with a pair of 80' Soller slits placed before and after the sample. For INS, a BeO low-pass filter was placed in front of the analyzer to remove higher order backgrounds. The measurement was performed only in the hhl scattering geometry.

In this manuscript, we describe the wave vectors in the hexagonal setting instead of the rhombohedral. As a result, the Bragg peaks will appear according to the reflection rule of $-h + k + l = 3n$. Although its Brillouin zone is three dimensional, it is convenient to use its two dimensional projection as shown in Fig. 1(b). We will show the spectra along high symmetry directions marked in Fig. 1(b) as well as the direction perpendicular to the honeycomb plane. Note that crystals belonging to the rhombohedral structure are typically subject to twin domains with different stacking sequences of the hexagonal planes. Neutron diffraction showed that the crystal used in this work is composed fully

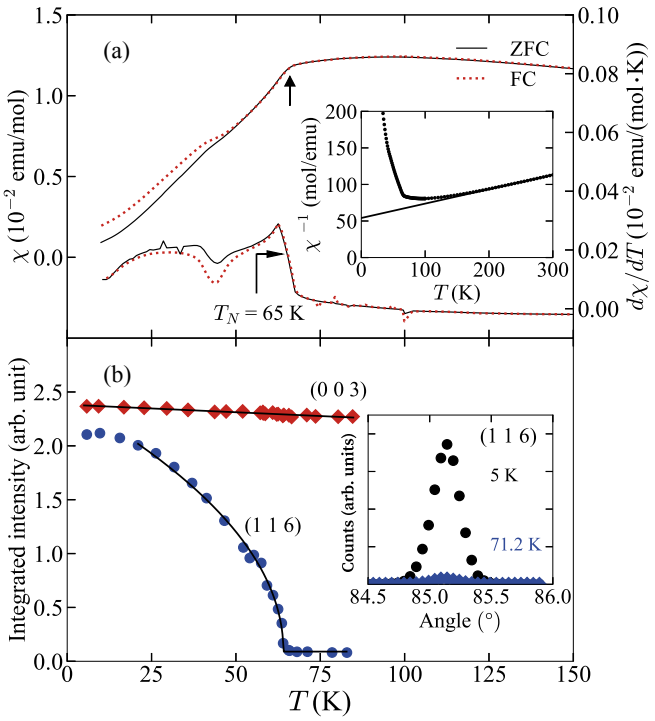

Fig. 2. (Color online) (a) Temperature dependencies of the field-cooled (red dashed line) and zero-field-cooled (black solid line) dc magnetic susceptibility ($\chi = M/B$) curves and their temperature derivatives ($d\chi/dT$). The inset shows the inverse susceptibility (χ^{-1}) and its Curie–Weiss fit over $240 \leq T \leq 300$ K. (b) Integrated intensities of the (003) and (116) Bragg peaks, respectively, measured by the neutron diffraction as the temperature was raised across T_N. The solid curve through the latter is the power law fit to the temperature-dependent component. The inset shows rocking scans of the (116) Bragg peak at $T = 5$ and 71.2 K, respectively.

of one structural twin. The mosaic spread was less than 0.5° in width. Although data are not shown, we also observed the incommensurate Bragg peaks at reported wave vectors.[12] These results confirm the high quality of the sample used in this work.

3. Results and Discussions

3.1 Antiferromagnetic phase transition of $MnTiO_3$

Figure 2(a) shows the dc magnetic susceptibilities along the c axis measured by the vibrating sample magnetometry below 300 K. Commonly in both FC and ZFC curves sharp downward turns are observed at $T_N = 65$ K indicating the onset of a long-range AFM ordering. Above T_N, however, a broad maximum is observed near ~100 K indicating deviations from a typical Curie–Weiss behavior. Such behavior is suggestive of dynamic short-range correlations consistently with the critical behavior near T_N.[20] We attempted to estimate the Curie–Weiss temperature by a linear fit to the inverse susceptibility between $240 \leq T \leq 300$ K since the deviation from the linearity was noticeable even up to 240 K. The fitted value of −272 K is probably less reliable than the earlier estimate of $|\Theta_{CW}| = 219$ K, which was obtained by fitting up to 600 K.[22] Below T_N, we also notice a split between the ZFC and FC susceptibility curves in spite of the seemingly robust long-range magnetic ordering. It suggests a small amount of disorder frozen in this temperature range. The temperature derivative of the susceptibility, $d\chi/dT$ also plotted in Fig. 2(a), reveals that the anomaly at 45 K appears commonly in both curves. Although having never explicitly

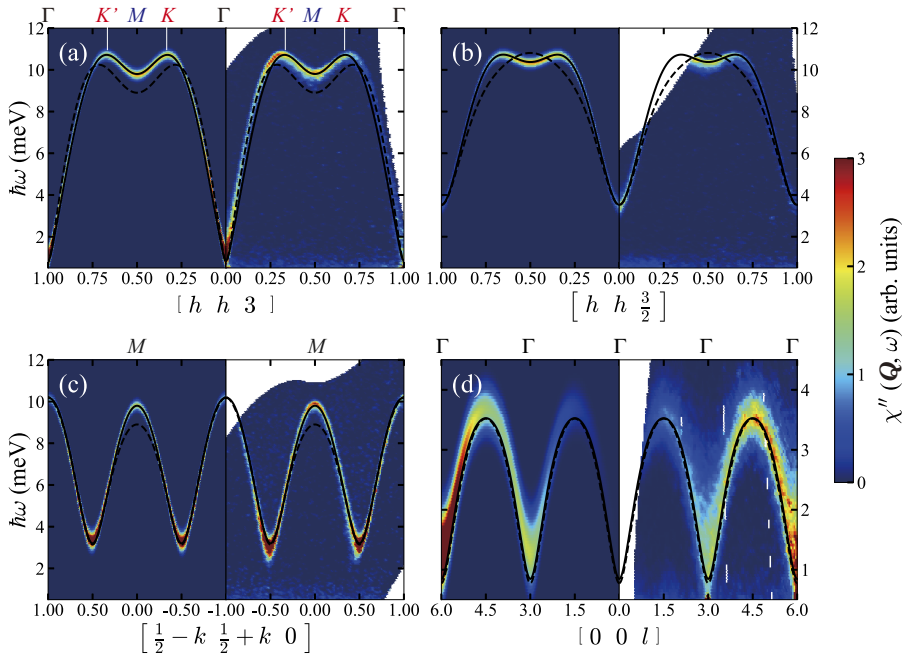

Fig. 3. (Color online) Right panels show the spin wave excitation spectra of $MnTiO_3$ observed at $T = 2$ K by the time-of-flight INS with $E_i = 15$ meV. The neutron scattering intensity was divided by the Bose factor to obtain the dynamic response function, $\chi''(\mathbf{Q}, \omega)$. Plotted in the left panels are the calculated $\chi''(\mathbf{Q}, \omega)$ using the constrained best-fit parameters listed in Table I and convoluted by the instrumental resolution. The solid lines are the dispersions calculated using the same parameters listed in Table I. For comparison, the dispersions calculated using the previously reported parameters[21] are shown with the dashed lines. The inelastic spectra on $\mathbf{Q} = (h - k, h + k, l)$ were integrated over the range of (a) $|k| \leq 0.04$ & $|l - 3| \leq 0.1$, (b) $|k| \leq 0.04$ & $|l - \frac{3}{2}| \leq 0.1$, (c) $|h| \leq 0.03$ & $|l| \leq 0.1$, and (d) $|h| \leq 0.03$ & $|k| \leq 0.04$.

been discussed, we find that this anomaly repeatedly showed up in the previous reports and is thus likely to be intrinsic to $MnTiO_3$.[11,13,20]

The onset of the long-range antiferromagnetic ordering was confirmed by observing the temperature dependence of magnetic Bragg peaks. Figure 2(b) shows that the intensity of the (116) Bragg peak consistently developed at T_N and continued to increase as the sample was cooled down. The integrated intensity can approximately be fitted with the power law, $I(T) \propto (T_N - T)^{2\beta}$, over a wide range excluding the low temperatures $T \leq 20$ K. The fitted exponent at $2\beta = 0.49$ is similar to the case of highly anisotropic Heisenberg magnets such as $MnPS_3$ or CrI_3.[28,29] In the mean time, the (003) Bragg peak did not show any changes in intensity across T_N indicating that the ordered magnetic moments are parallel to the c axis. These data commonly suggest that $MnTiO_3$ in the Néel phase involves a small degree of instability ascribable to its pseudo-2D nature.

3.2 Spin waves of $MnTiO_3$ at $T = 2$ K

To understand the antiferromagnetic spin dynamics in $MnTiO_3$, we investigated the spin wave excitations over a wide temperature range covering below and above T_N. To accurately estimate both of the in-plane and out-of-plane exchange interactions, the data at $T = 2$ K were obtained from two different scattering geometries discussed previously. In Fig. 3 we show the $\mathbf{Q} - \hbar\omega$ slices of the inelastic neutron scattering data cut along the representative directions in the reciprocal space. The experimental data on each panel are directly compared with model calculations, which are to be discussed soon. The overall momentum dependence of the spin wave energy is apparently consistent with typical honeycomb Heisenberg antiferromagnets with strong nearest neighbor AFM exchanges.[30,31] As shown in Fig. 3(a), the magnon energy extended up to the maximum value of 10.7 meV at $\mathbf{Q}_K = (\frac{1}{3}, \frac{1}{3}, 3)$ and $\mathbf{Q}'_K = (\frac{2}{3}, \frac{2}{3}, 3)$, which correspond to the corners of the two dimensional Brillouin zone boundaries shown Fig. 1(b). The dispersion along $[h\ h\ 3]$ direction is symmetric about the middle point at $\mathbf{Q}_M = (\frac{1}{2}, \frac{1}{2}, 3)$. At the same time, the minimum energy of $E_g \approx 0.8$ meV is observed at $\mathbf{Q}_\Gamma = (0, 0, 3)$ consistently with the previous work.[21] The finite energy gap at the Brillouin zone center is ascribed to the single-ion easy-axis anisotropy field along the c axis.

From the data plotted in Fig. 3(b), we also find that the overall in-plane wave vector dependence is similar between two directions of $[h\ h\ l]$ with $l = 3$ and $\frac{3}{2}$, respectively. The apparent differences are ascribed to the fact that with $l = \frac{3}{2}$ none of the wave vectors included in Fig. 3(b) exactly correspond to the high symmetry points marked in Figs. 3(a) and 1(b). In particular, the large difference between their minimum energies indicates that the out-of-plane exchange interactions have significant strength. Indeed, Fig. 3(d) shows that along the $[0\ 0\ l]$ direction the spin wave energy reaches up to 3.5 meV, which is as large as one third of the in-plane band width. It suggests that the AFM ordering of $MnTiO_3$ is far from being two dimensional at low temperatures.

Figure 3(c) shows the spin waves along the other in-plane high symmetry direction that is crossing $\mathbf{Q}_M$. When combined with the data in Fig. 3(a), a saddle point of the spin wave band structure is identified at $\mathbf{Q}_M$, where the curvature of $\hbar\omega(\mathbf{Q})$ is opposite in signs between the two mutually orthogonal in-plane directions: $[h\ h]$ and $[-k\ k]$, respectively. We find that such saddle-point-like band topology appear independently of the l index.

Table I. The exchange and anisotropy constants obtained by the least square fitting of the spin wave excitations observed at $T = 2$ K. The parameters were constrained to be $J_1 + 2J_2 + J_3 = 2.1$ meV as discussed in the text. The size of spin moment was assumed to be $S = 5/2$.

	J_1	J_2	J_3	J_{c1}	J_{c2}	J_{c3}	D
strength (meV)	1.833	0.139	−0.012	0.507	0.131	0.127	0.0045
length (Å)	3.03	5.12	5.95	4.09	5.61	6.20	—

To accurately estimate the exchange energies, we performed the least square fitting of the experimental data using the calculations based on the standard Holstein–Primakoff linearization method.[32] We used the spin Hamiltonian including three in-plane (J_1, J_2, & J_3) and three out-of-plane (J_{c1}, J_{c2}, & J_{c3}) isotropic Heisenberg exchanges which are depicted in Fig. 1(a). Additionally, we also included an easy-axis anisotropy constant D along the c axis. The spin Hamiltonian is thus written as follows:

$$H = \frac{1}{2}\sum_{i\neq j} J_{ij}\mathbf{S}_i \cdot \mathbf{S}_j - \sum_j D_j(\mathbf{S}_j \cdot \mathbf{c})^2. \quad (1)$$

While the above Hamiltonian was originally proposed for $MnTiO_3$,[21] the parameters reported in the previous work largely failed to reproduce the spin wave energies near the top of the band. As shown with dashed lines in Fig. 3(b), the disagreement is particularly noticeable along the $[h\ h\ \frac{3}{2}]$ direction, which suggests an overestimation of interplanar exchanges.

In our analysis, we constrained the sum of the three in-plane exchange constants using on the Curie–Weiss temperature: $J_{\mathrm{CW}} \equiv 3J_1 + 6J_2 + 3J_3 = 3k_{\mathrm{B}}|\Theta_{\mathrm{CW}}|/[S(S+1)(g-1)^2] = 6.3$ meV.[31] This constraint is based on the assumption that the magnetic interactions are virtually two dimensional at $T \gg T_{\mathrm{N}}$, which will eventually be confirmed. The best-fit parameters obtained using this constraint are listed in Table I, and the calculated dispersions are plotted as solid lines in Fig. 3. Also plotted in the left panels of Fig. 3 are the calculated neutron scattering intensities using the same best-fit parameters that are directly compared with the experimental data on the right panels. We find that J_1 along the shorted Mn–Mn bond is antiferromagnetic and the largest in magnitude consistently with the edge-sharing geometry of the nearest-neighbor MnO_6 octahedra, which allows direct exchange of Mn^{2+} t_{2g} electrons. Note that the rest of the bonds must go through O^{2-} $2p$ orbitals. We also find that J_3 is particularly weak as expected from its extended path around the honeycomb hexagon.

In contrast, we find that the second largest exchange is J_{c1} ($= 0.28J_1$) along the shortest out-of-plane bonds. As shown in Table I, among the three interplanar exchanges the strengths of J_{c2} and J_{c2}, respectively, are approximately 25% of J_{c1}. These results confirm that that J_{c2} and J_{c2} had been overestimated in the previous work.[21] However, the dimensionality of the magnetic interactions should be assessed from the ratio between the net interplanar ($J_c \equiv J_{c1} - 6J_{c2} + 3J_{c3}$) and intraplanar ($J_{ab} \equiv 3J_1 - 6J_2 + 3J_3$) exchange couplings.[21] Note that J_{ab} in the AFM ordered phase is different from J_{CW} of the paramagnetic phase because the former should consider the relative orientations of the spin vectors. For the same reason, the value of J_c is also reduced when all three interplanar exchanges are AFM with the same signs. We obtain $J_c/J_{ab} = 0.022$ from our best-fit parameters, which is consistent with the previous picture that the exchange cancellations due to the six-folded J_{c2} leads to significant weakening of J_c.[21] While the estimated ratio is smaller by factor two than the previous report,[21] we suppose that it is still not sufficiently small to make $MnTiO_3$ a two dimensional magnet. For comparison, this ratio is reported to be as small as $J_c/J_{ab} \sim 10^{-4}$ in a planar honeycomb antiferromagnet $BaNi_2V_2O_8$.[31] We thus look for a clue in the temperature dependence of the exchange asymmetry in the following section.

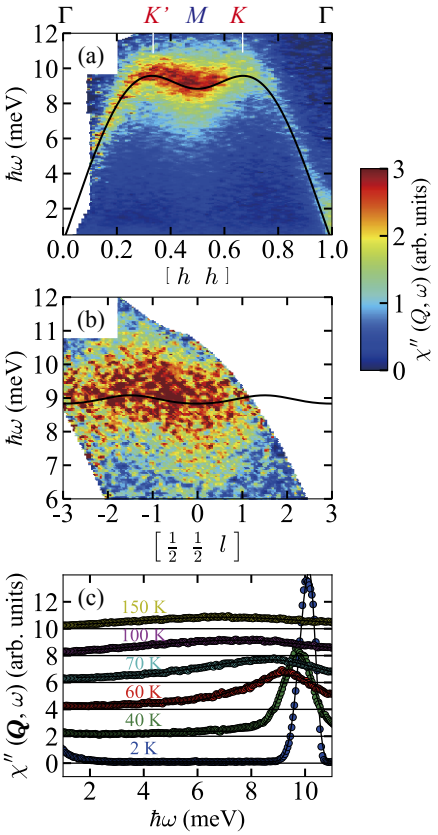

Fig. 4. (Color online) Magnetic excitation spectra of $MnTiO_3$ observed at $T = 60$ K along (a) $[h\ h\ 0]$ and (b) $[\frac{1}{2}\ \frac{1}{2}\ l]$ directions, respectively. The solid lines are the linear spin wave calculation using the best-fit parameters obtained at 60 K. The panel (c) shows the temperature dependence of the spectra at $\mathbf{Q} = (\frac{1}{2}, \frac{1}{2}, 0)$. The integrated ranges of the spectra on $\mathbf{Q} = (h-k, h+k, l)$ are (a) $|k| \leq 0.04$ & $|l| \leq 3$, (b) $|h - \frac{1}{2}| \leq 0.03$ & $|k| \leq 0.04$, and (c) $|h - \frac{1}{2}| \leq 0.06$, $|k| \leq 0.04$, & $|l| \leq 3$, respectively.

Before turning to the temperature dependence, we comment on the possibility of the antisymmetric Dzyaloshinkii–Moriya (DM) exchange coupling in the spin dynamics of $MnTiO_3$. In the honeycomb lattice of the $R\bar{3}$ space group, the inversion symmetry prevents DM coupling across the nearest neighbor bonds. Instead, finite DM terms are allowed across the next nearest neighbor bonds, which will cause an inequality between magnon energies at $\mathbf{Q}_K$ and $\mathbf{Q}_{K'}$, respectively.[33] We note that there is no evidence of the DM coupling larger than 10^{-3} meV in our data.

3.3 *Temperature dependence of the spin waves on $MnTiO_3$*

To understand how the magnetic exchange interactions in $MnTiO_3$ evolve with temperature, we repeated the INS measurements at elevated temperatures near and above T_{N}. Figure 4(a) shows the excitation spectra at $T = 60$ K

($= 0.95T_N$) along the in-plane [h h] direction. It is apparent that the spin wave band width decreased only by ∼10% with respect to $T = 2$ K although the excitations became significantly broad in energy. Note that the full dispersion of the in-plane modes is still observable exhibiting the energy maxima at $\mathbf{Q}_K$ and $\mathbf{Q}_{K'}$, respectively, and the minimum at $\mathbf{Q}_M$. It suggests that the in-plane exchanges, or J_{ab}, remain strong even at temperatures close to T_N. At the same time, the l-dependent dispersion at the high energy was also noticeable although it became significantly flatter [see Fig. 4(b)]. When the temperature was further increased to above T_N, the in-plane modes became hardly observable with significant weight shifting to lower energies. However, the center of the spectral weight remained at finite energies even at $T = 150$ K ($= 2.3T_N$) well above T_N [see Fig. 4(c)].

To better understand the temperature dependencies of the interplanar exchanges and the anisotropy field, we used the triple-axis spectroscopy and measured the spin wave energies at $\mathbf{Q}_\Gamma = (0, 0, 3)$ and $\mathbf{Q}_Z = (0, 0, 4.5) = \mathbf{Q}_\Gamma + (0, 0, \frac{3}{2})$, respectively. These two wave vectors correspond to the minimum and maximum, respectively, of the spin wave dispersion along the [0 0 l] direction. Figure 5(a) shows that the anisotropy gap at $\mathbf{Q}_\Gamma$ gradually decreases from $E_g = 0.8$ meV at $T = 5$ K to $\lesssim 0.2$ meV at $T = 64.2$ K ($\approx T_N$). Above T_N, the gap apparently vanishes under the current experimental resolution. Meanwhile the out-of-plane band width observed at $\mathbf{Q}_Z$ is reduced by ∼40% over the same temperature range. We note that the spin wave at a finite energy is still observable at $T = 64.2$ K as shown in Fig. 5(b). The spin wave peak persisted up to ≈70 K, beyond which the scattering intensity became featureless. The detailed temperature dependencies at these two wave vectors are summarized in Fig. 5(c).

Since the apparent spin wave energies depend simultaneously on J_{ab}, J_c, and D, the temperature dependence of each parameter were extracted by performing the least square fittings at different temperatures. We assumed that the internal ratios among in-plane ($J_1 : J_2 : J_3$) and out-of-plane ($J_{c1} : J_{c2} : J_{c3}$) exchanges, respectively, remain unchanged as the temperature increased, and fitted only J_{ab}, J_c, and D as variable parameters. For instance, the best fit parameters obtained at $T = 60$ K were used to calculate the solid lines in Fig. 4. We finally plotted in Fig. 5(d) the three parameters respectively normalized to the values at $T = 2$ K. It shows that the easy-axis anisotropy decreases towards T_N following almost linear dependence on temperature. When fitted with the power law, $D(T) \propto (T_N - T)^\eta$, its critical exponent is found to be $\eta \approx 0.8$. Since we fixed $S = 5/2$ in the spin Hamiltonian, the effect of reduced ordered moments should be included in the numerical values of the fitted parameters. Comparison with the temperature dependence of the sublattice magnetization ($\beta = 0.25$) in Fig. 2(b) reveals that the anisotropy field decreases much faster than the sublattice magnetization. It clearly shows that local anisotropy field plays a crucial role in stabilizing long-range magnetic order. In contrast, J_{ab} and J_c could not be fitted with the power laws but instead remain finite near T_N. While J_{ab} changed only by ∼10% up to T_N, however, J_c more significantly decreased by ∼60% in the same temperature range. While J_c evidently remains finite at T_N, it clearly suggests that the magnetic interactions in $MnTiO_3$ becomes more anisotropic at high temperatures. The quadratic fit used as a guide to the eye shown in Fig. 5(d) suggests that J_c will eventually become negligible near $T \approx 90$ K justifying the earlier assumption of two dimensional magnetic interactions at high temperatures. This result is also consistent with the crossover in dimensionality from 3D to 2D observed earlier by quasi-elastic scattering.[20)]

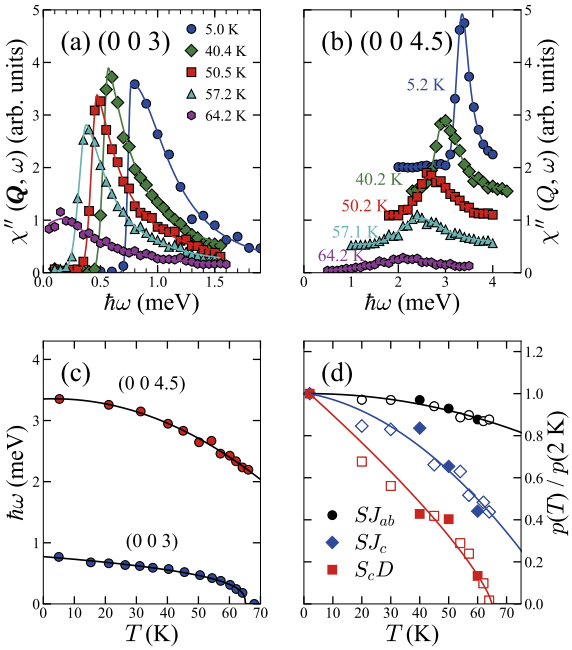

Fig. 5. (Color online) Temperature dependencies of the dynamic response function observed at (a) $\mathbf{Q} = (0, 0, 3)$ and (b) $(0, 0, 4.5)$. The solid lines through data are fits using the phenomenological asymmetric functions combining Gaussian and Lorentzian line shapes. The fitted peak positions are plotted in (c). (d) Temperature dependences of the effective in-plane exchange (J_a), out-of-plane exchange (J_{ab}), and the easy-axis anisotropy (D) constants. The solid lines through data are guides to the eye.

4. Conclusion

In summary, we report the temperature dependence of the spin wave excitations in the honeycomb antiferromagnet $MnTiO_3$ using high-resolution inelastic neutron scattering. By fitting with the linear spin wave calculations, we provide the spin Hamiltonian that can accurately reproduce spin wave energies over the entire Brillouin zone at $T = 2$ K. It shows that the magnetic interactions at low temperatures are only marginally 2D with the net interplanar exchange to be ∼2% of the net intraplanar one. As the temperature is increased up to T_N, we find that the interplanar exchange decreases more rapidly than the intraplanar exchange, and thereby the magnetic interaction becomes more anisotropic. We deduce that the magnetic interactions in $MnTiO_3$ should finally cross over from being 3D to 2D at ∼90 K within the paramagnetic phase above T_N.

Acknowledgments This work was supported by the National Research Foundation (NRF) of Korea (Grant Nos. 2020R1A5A1016518 and 2020K1A3A7A09077712). K.I. thanks for the travel expense supprt from ISSP, Univ. Tokyo. This research used resources at the Spallation Neutron Source, a DOE Office of Science User Facility operated by the Oak Ridge National Laboratory. The authors acknowledge the support of the National Institute of Standards and Technology, U.S. Department of Commerce, in providing the neutron research facilities used in this work.

*jaehc@korea.ac.kr
†s_shamoto@cross.or.jp

1) W. Eerenstein, N. D. Mathur, and J. F. Scott, Nature **442**, 759 (2006).
2) S.-W. Cheong and M. Mostovoy, Nat. Mater. **6**, 13 (2007).
3) N. Ortega, A. Kumar, J. F. Scott, and R. S. Katiyar, J. Phys.: Condens. Matter **27**, 504002 (2015).
4) T. Kimura, T. Goto, H. Shintani, K. Ishizaka, T. Arima, and Y. Tokura, Nature (London) **426**, 55 (2003).
5) H. Katsura, N. Nagaosa, and A. V. Balatsky, Phys. Rev. Lett. **95**, 057205 (2005).
6) M. Mostovoy, A. Scaramucci, N. A. Spaldin, and K. T. Delaney, Phys. Rev. Lett. **105**, 087202 (2010).
7) Y. S. Oh, S. Artyukhin, J. J. Yang, V. Zapf, J. W. Kim, D. Vanderbilt, and S.-W. Cheong, Nat. Commun. **5**, 3201 (2014).
8) R. Saha, S. Ghara, E. Suard, D. H. Jang, K. H. Kim, N. V. Ter-Oganessian, and A. Sundaresan, Phys. Rev. B **94**, 014428 (2016).
9) A. Maignan and C. Martin, Phys. Rev. Mater. **2**, 091401(R) (2018).
10) H. Toyosaki, M. Kawasaki, and Y. Tokura, Appl. Phys. Lett. **93**, 072507 (2008).
11) N. Mufti, G. R. Blake, M. Mostovoy, S. Riyadi, A. A. Nugroho, and T. T. M. Palstra, Phys. Rev. B **83**, 104416 (2011).
12) H. J. Silverstein, E. Skoropata, P. M. Sarte, C. Mauws, A. A. Aczel, E. S. Choi, J. van Lierop, C. R. Wiebe, and H. Zhou, Phys. Rev. B **93**, 054416 (2016).
13) R. K. Maurya, N. Singh, S. K. Pandey, and R. Bindu, Europhys. Lett. **110**, 27007 (2015).
14) G. Shirane, S. J. Pickart, and Y. Ishikawa, J. Phys. Soc. Jpn. **14**, 1352 (1959).
15) H. Kato, S. Funahashi, Y. Yamaguchi, M. Yamada, and H. Takei, J. Magn. Magn. Mater. **31–34**, 617 (1983).
16) R. E. Newnham, J. H. Fang, and R. P. Santoro, Acta Crystallogr. **17**, 240 (1964).
17) S. Chi, F. Ye, H. D. Zhou, E. S. Choi, J. Hwang, H. Cao, and J. A. Fernandez-Baca, Phys. Rev. B **90**, 144429 (2014).
18) S. W. Chen, P. A. Lin, H. T. Jeng, S. W. Fu, J. M. Lee, J. F. Lee, C. W. Pao, H. Ishii, K. D. Tsuei, N. Hiraoka, D. P. Chen, S. X. Dou, X. L. Wang, K. T. Lu, and J. M. Chen, Appl. Phys. Lett. **104**, 082104 (2014).
19) A. Fukaya, A. Ito, H. A. Katori, and T. Goto, J. Phys. Soc. Jpn. **69**, 3027 (2000).
20) J. Akimitsu and Y. Ishikawa, J. Phys. Soc. Jpn. **42**, 462 (1977).
21) Y. Todate, Y. Ishikawa, K. Tajima, S. Tomiyoshi, and H. Takei, J. Phys. Soc. Jpn. **55**, 4464 (1986). The sum of in-plane exchange constants obtained in this work ($J_1 + 2J_2 + J_3 = 1.4$ meV) suggests $|\Theta_{CW}| = 144$ K, which is too small.
22) J. J. Stickler, S. Kern, A. Wold, and G. S. Heller, Phys. Rev. **164**, 765 (1967).
23) E. Rastelli, A. Tassi, and L. Reatto, Physica B **97**, 1 (1979).
24) J. B. Fouet, P. Sindzingre, and C. Lhuillier, Eur. Phys. J. B **20**, 241 (2001).
25) H. Takei, J. Mater. Sci. **16**, 1310 (1981).
26) B. Winn, U. Filges, V. O. Garlea, M. Graves-Brook, M. Hagen, C. Jiang, M. Kenzelmann, L. Passell, S. M. Shapiro, X. Tong, and I. Zaliznyak, EPJ Web Conf. **83**, 03017 (2015).
27) I. A. Zaliznyak, A. T. Savici, V. Ovidiu Garlea, B. Winn, U. Filges, J. Schneeloch, J. M. Tranquada, G. Gu, A. Wang, and C. Petrovic, J. Phys.: Conf. Ser. **862**, 012030 (2017).
28) A. R. Wildes, H. M. Rønnow, B. Roessli, M. J. Harris, and K. W. Godfrey, Phys. Rev. B **74**, 094422 (2006).
29) Y. Liu and C. Petrovic, Phys. Rev. B **97**, 014420 (2018).
30) D. E. McNally, J. W. Simonson, J. J. Kistner-Morris, G. J. Smith, J. E. Hassinger, L. DeBeer-Schmitt, A. I. Kolesnikov, I. A. Zaliznyak, and M. C. Aronson, Phys. Rev. B **91**, 180407(R) (2015).
31) E. S. Klyushina, B. Lake, A. T. M. N. Islam, J. T. Park, A. Schneidewind, T. Guidi, E. A. Goremychkin, B. Klemke, and M. Månsson, Phys. Rev. B **96**, 214428 (2017).
32) S. Toth and B. Lake, J. Phys.: Condens. Matter **27**, 166002 (2015).
33) S. A. Owerre, J. Appl. Phys. **121**, 223904 (2017).